AIMS Materials Science, 7(3): 288–301.
DOI: 10.3934/matersci.2020.3.288
Received: 05 April 2020
Accepted: 03 June 2020
Published: 04 June 2020

http://www.aimspress.com/journal/Materials

Research article

Magnetite nanoparticles-TiO_2 nanoparticles-graphene oxide nanocomposite: Synthesis, characterization and photocatalytic degradation for Rhodamine-B dye

Khang Duy Vu Nguyen[1] and Khoa Dang Nguyen Vo[1,2,*]

[1] Institute of Applied Materials Science, Vietnam Academy of Science and Technology, 01A TL29 Street, Thanh Loc Ward, District 12, Ho Chi Minh City 700000, Vietnam
[2] Graduate University of Science and Technology, Vietnam Academy of Science and Technology, 18 Hoang Quoc Viet Street, Nghia Do Ward, Cau Giay District, Ha Noi 100000, Vietnam

* **Correspondence:** Email: vndkhoa@iams.vast.vn; Tel: +84909622589.

Abstract: Herein, a ternary nanocomposite of magnetite nanoparticles (MNPs), TiO_2 nanoparticles (TNPs), and graphene oxide (GO) (Fe_3O_4@TiO_2/graphene oxide, GMT) has been successfully synthesized for photocatalytic degradation of rhodamine B (RhB) dye under natural sunlight irradiation, which is a significant elevation in photocatalytic activity and sustainability for both Fe_3O_4@TiO_2 nanoparticles and magnetic GO materials. MNPs was first incorporated with TNPs to form Fe_3O_4@TiO_2 core/shell nanoparticles, followed by the addition of GO. The nanocomposite's morphological, chemical and physical properties were investigated through various spectroscopic techniques such as Fourier-transformed infrared (FTIR), X-ray diffraction (XRD), and ultraviolet-visible (UV-Vis) adsorption. Vibrating-sample magnetometry, Brunauer-Emmett-Teller (BET) equation, scanning electron (SEM), and transmission electron (TEM) microscopies were also used for the nanocomposite formation demonstration. In comparison with bare components, GMT samples displayed much higher degradation efficiency on rhodamine B (RhB) dye solutions under natural sunlight irradiation. The nanocomposite, therefore, proclaimed high potential as a "next-step" material of Fe_3O_4@TiO_2 core/shell nanoparticles for pollutants removal from wastewater and other photocatalytic applications.

Keywords: graphene oxide; titanium dioxide; magnetite nanoparticles; nanocomposites; photocatalytic activity

1. Introduction

With the significant development of industry, environmental pollution has become a hot topic in the world, particularly the contamination of water sources and wastewaters due to the release of heavy metals, organic dyes, oil spills, and so on [1,2]. Such contaminants present toxicity and constitute serious threats to both human and environmental health. It is, therefore, of great significance to design efficient and environmental friendly techniques for the purification of wastewater [3,4]. Semiconductor-based heterogeneous photocatalysis is one of the most promising alternatives for the management and remediation of contaminated water. Among available catalyst platforms, titanium dioxide (TiO_2) is regarded as one of the most widely accepted photocatalysts for the degradation of pollutants in aqueous solutions [5,6]. This superiority of TiO_2 is attributed to its numerous advantages such as chemically and biologically inert, photo-catalytically stable, capable of efficiently catalyzing reactions, relatively easy to produce and use, low-cost and entirely risk-free to humans and the environment [7,8]. However, TiO_2 could only be photo-excited under ultraviolet (UV) light irradiation due to its wide band-gap of 3.2 eV, which is unsuitable for natural light catching and for transition electrons from valence band to conduction band. The high rate of recombination of photo-generated electron-hole pairs in TiO_2 leads to reduction in photocatalytic efficiency [9,10]. On the other hand, good dispersion of TiO_2 in water remains shortcoming for this material to be collected after use. To overcome these obstacles, typical photocatalysts have been extensively modified by doping TiO_2 with metals [11,12], non-metals [13], and/or rare earth minerals [14], and mixing TiO_2 with other nanomaterials [15].

A typical metal oxide nanoparticles with superparamagnetic activity, magnetite (Fe_3O_4) nanoparticles (MNPs) possesses great interest for industrial, environmental, biological and medicinal applications [16]. This material is biocompatible and very low-cost, allowing it to be produced in large scale and used for human with undeniable safe. In human body, iron from degraded iron oxide nanoparticles enters the natural iron store such as hemoglobin in red blood cells. The superparamagnetic activity, chemical stability, and low toxicity of Fe_3O_4 nanoparticles contribute to its wide application in industrial and environmental domains. The high ratio surface to volume of magnetite nanoparticles results in a higher adsorption capacity for metal removal, hence its high potential as "metal and organic remover" for wastewater [17]. Moreover, magnetite nanoparticles are combined with other nanomaterials for the enhancement of both its photocatalytic activity and the post-treatment collectability of others [18,19].

Combination of Fe_3O_4 and TiO_2 as core-shell nanocomposites, especially nanoparticles (Fe_3O_4@TiO_2), have been studied. Photocatalytic activity of such nanocomposites were demonstrated higher than their sole components. In addition, Fe_3O_4@TiO_2 nanoparticles were much easier to be collected after usage, thanks to the superparamagnetic property of magnetite. Their applications, therefore, have been considerably expanded [20–24]. Besides, magnetite nanoparticles have been mingled with graphene-based materials, such as graphene or reduced graphene oxide (rGO), forming "magnetic graphenes". These materials exhibits desirable magnetic response, hence their wide application in magnetic energy storage, fluids or catalysis [25]. Graphene oxide (GO) has a similar structure to graphene, except the presence of oxygen-containing functional groups such as hydroxyl (–OH), epoxy and alkoxy (C–O–C), carboxylic (–COOH), carbonyl (C=O), and so forth [26]. Apart from the ease of preparation, the presence of oxygenated groups is answerable for advantages over graphene or reduced graphene oxide, including higher solubility and the effectiveness of surface

modification [27]. Graphene and reduced graphene oxide were used to form nanocomposites with Fe_3O_4@TiO_2 nanoparticles in previous studies [21,28] and these materials were demonstrated possessing fascinating photocatalytic activity. With distinct structural advantages over graphene and reduced graphene oxide, graphene oxide (GO) is absolutely capable of forming stable bonds with TiO_2 and Fe_3O_4, hence the very high potential of its nanocomposite descendant for photocatalytic and environmental applications.

In this study, photocatalytic and recovery advantages of both Fe_3O_4@TiO_2 nanoparticles and magnetic graphene-based materials were evaluated by the combination of Fe_3O_4@TiO_2 nanoparticles and GO sheets. Fe_3O_4@TiO_2 core-shell nanoparticles and GO sheets were synthesized separately, followed by their chemical mixing with GO, to form Fe_3O_4@TiO_2-GO nanocomposite. Morphological, physical and chemical properties of the nanocomposite were investigated using Fourier-transformed (FTIR), X-ray diffraction (XRD) and ultraviolet-visible (UV-Vis) adsorption spectroscopies; scanning electron and transmission electron (TEM) microscopies, as well as vibrating-sample magnetometry and Brunauer-Emmett-Teller (BET) equation. In order to clarify the way in which MNPs, TNPs and GO bonds with each other, different weight ratios of these ingredients were applied and investigated. The nanocomposites' photocatalytic activity was evaluated by the photodegradation of rhodamine B (RhB) dye solution under natural sunlight exposure, comparing with the sole components (GO, MNPs and TNPs). With such combinations, Fe_3O_4@TiO_2-GO nanocomposite is expected to be a promising "offspring" of Fe_3O_4@TiO_2 nanoparticles and magnetic graphene-based materials for application in wastewater purification and other photocatalytic fields.

2. Materials and methods

2.1. Materials

Graphite powder was purchased from ACROS Organics (Nidderau, Germany). Tetrabutyl orthotitanate (TBOT) was obtained from MERCK (Darmstadt, Germany). Magnetite nanopowder (50–100 nm particle size) was purchased from Sigma-Aldrich (St. Louis, United States), and rhodamine B (RhB) dye was obtained from HiMedia (Mumbai, India). All other chemicals were in analytical grade and used without further purification throughout the study.

2.2. Preparation of graphene oxide (GO)

GO was synthesized using conventional Hummer's technique [29], but with the amount of all ingredients originated from Marcano's publication [30]. 69 mL of concentrated H_2SO_4 was added to a 250 mL Erlenmeyer flask containing a mixture of graphite powder (3.0 g) and $NaNO_3$ (1.5 g). The mixture was constantly stirred, stored in a fridge until it reached to 0oC, and then continuously stirred in an ice bath. $KMnO_4$ (9.0 g) was added to the mixture and then the reaction temperature was maintained less than or equal to 20 ºC. When $KMnO_4$ was completely added, the oxidation of graphite was occurred, leading to the formation of NO_2 and a light red-brown suspension. The mixture was further vigorously stirred with a glass chopstick for approximately 30 min, in which its colour turned to grey. 138 mL of deionized water was gently added, at which time the reaction released a large exotherm up to 98 ºC. Such reaction temperature was maintained using external

heating for 15 min. The mixture was cooled down using a water bath, followed by the addition of deionized water (420 mL) and 30% H_2O_2 (3 mL), which later produced another exotherm and effervescence. Thus the mixture was continuously stirred, cooled down again, and purified by filtration and multi-washings with deionized water, HCl 10 % and ethanol, respectively, followed by centrifugation and vacuum drying to obtain the final product.

2.3. Synthesis of Fe_3O_4@TiO_2 core-shell nanoparticles

Fe_3O_4 nanopowder was dispersed in 50 mL of deionized water in a three-necked round flask for 15 min using sonication. The flask was then fit to a mechanical stirrer equipped with a Teflon propeller. The suspension was vigorously stirred for 5 min and slightly heated to 45n ºC. After that, TBOT (0.1 mol·L^{-1}) and H_3BO_3 solution (0.3 mol·L^{-1}) were added with continuous vigorous stirring for 30 min, followed by the addition of 10 mL of NH_4OH (5.44 mol·L^{-1}) and then 3 mL of H_2O_2 30% (wt%). The flask was sealed, heated to 95 ºC and the suspension was left stirred vigorously for 5 h. After 5 h, the suspension progressed to the addition of GO solution for the synthesis of Fe_3O_4@TiO_2-GO nanocomposite.

2.4. Synthesis of Fe_3O_4@TiO_2-GO nanocomposite and physical mixtures

Before the finish of Fe_3O_4@TiO_2 nanoparticles' formation, the GO suspension was prepared by dispersing GO in 40 mL of deionized water for 15 min using sonication. After the Fe_3O_4@TiO_2 suspension was completely synthesized, the flask was unsealed and then the GO dispersion was added dropwise with continuous vigorous stirring. The flask was then resealed, heated to 110 ºC and the suspension was left stirred vigorously for another 2 h. After 2 h, the suspension was isolated from heat and the product was collected using a magnet and then followed by multiple deionized water-washing until the pH value reached 7.0 to 7.5 to obtain the Fe_3O_4@TiO_2-GO nanocomposite (or GMT) product as dark grey powder.

The weight ratio between GO, Fe_3O_4 and TiO_2 was investigated in three values: GO:Fe_3O_4:TiO_2 1:1:1, 2:1:1, and 2:1:2, and the obtained products were labelled GMT 111, GMT 211 and GMT 212, respectively. The physical mixtures of GO, Fe_3O_4 and TiO_2 nanoparticles, with the same weight ratios as used for the nanocomposites' synthesis, were prepared simply by direct mixing of GO, Fe_3O_4 and TiO_2 nanoparticles, namely GMT 111M, GMT 211M and GMT 212M, respectively.

2.5. Characterizations

The values regarding magnetic property of nanocomposites were obtained on a MicroSense EasyVSM magnetometer (MicroSense, Massachusetts, United States) and the BET experiments were conducted on a Micromeritics TriStar 3000 analyser (Micromeritics, Georgia, United States). FTIR spectroscopy was recorded on a Perkin-Elmer MIR/NIR Frontier spectrometer (PerkinElmer, Waltham, Maryland, United States) in the wavenumber range of 400–4000 cm^{-1} using KBr pellets. For XRD patterns, a Bruker D2 Phaser spectrometer (Bruker, Massachusetts, United States) was used, with Cu K-α as radiation source (λ= 1.5418 Å, 40 kV, 25 mA) and scanning speed of 0.5°/min in the 2θ range of 10–80°. UV-Vis absorption spectra were recorded on an UV-1800 spectrometer (SHIMADZU, Kyoto, Japan). The morphology of all samples was observed by an S-4800 FESEM

microscope (HITACHI, Ibaraki, Japan) for SEM imaging and a JEM-1400 TEM microscope (JEOL, Maryland, United States) for TEM imaging.

2.6. Photocatalytic activity investigation

Before photocatalytic experiments, proportion of Fe_3O_4 and TiO_2 in GMT samples were determined by inductively coupled plasma mass spectrometry (ICP-MS), on a NexION®2000 spectrometer (PerkinElmer, Waltham, Maryland, United States). Subsequently, proportion of GO was calculated based on that of Fe_3O_4 and TiO_2 obtained previously. All GMT samples were dissolved in hot solution of HNO_3/HF mixture so that Fe_3O_4 and TiO_2 were transformed to soluble salts. The solutions were then diluted with deionized water for ICP-MS analysis. The highest proportion value of GO, Fe_3O_4, and TiO_2 were applied for determination of appropriate amount of bare components for photocatalytic activity investigation.

Aqueous solutions of RhB (10 $mg \cdot L^{-1}$) were used as targets for photocatalytic reactions. Subsequently, the material was added to the RhB solutions, constantly stirred for 20 min in the dark so that the adsorption equilibrium could be fully established. The samples were kept stirring under natural sunlight irradiation for 1 h. In this context, all experiments were conducted at around 11 a.m., when light conditions were the most intact. After 1 h, the solutions were isolated from shining sunlight to prevent continuous degradation of dyes and later centrifuged to remove catalyst particles completely. The obtained solutions were characterized by an UV-1800 spectrophotometer (SHIMADZU, Kyoto, Japan) at wavelength range of 200–900 nm.

The UV-Vis adsorption spectra of RhB solutions (0 to 10 $\mu g \cdot mL^{-1}$) without photocatalysts were also conducted to create the calibration curve of RhB (determined as $y = 0.226388x + 0.0142417$; $R2 = 0.99950$), which was then applied to calculate the decolouration efficiency of all samples, following the formula of $D\ (\%) = [(C0 - C)/C0] \times 100$. Whereas D is decolouration efficiency, C0 and C ($mg \cdot L^{-1}$) is the initial and equilibrium concentrations of RhB. At center time intervals, the samples (4 mL) were filtered through polyvinylidene difluoride (PVDF) membranes (pore size at 0.22 μm) and then measured the absorbance at $\lambda = 554$ nm with UV-visible spectrophotometer. For the verification of RhB concentration decreasing manner of GMT and bare components samples, an Agilent 100 HPLC system equipped with UV-Vis detector was used.

2.7. Statistical analysis

The data were expressed as mean ± standard deviation. The statistical data evaluation was performed using Microsoft®Excel.

3. Results and discussion

3.1 Characterization of Fe_3O_4@TiO_2-GO (GMT) nanocomposites

The FTIR spectra (Figure 1) indicated the presence of GO, MNPs and TNPs components in all GMT samples. For details, signals of GO at ~3400 cm^{-1} (OH groups), ~1600 cm^{-1} (carbonyl groups) [31]; TiO_2 at ~3400 cm^{-1} (OH groups); ~1600 cm^{-1} and ~600 cm^{-1} (Ti–O bonds) [32]; Fe_3O_4 at ~3400 cm^{-1} (OH groups); ~600 cm^{-1} (Fe–O bonds) [33] could be observed clearly in all GMT

samples. In addition, the spectra of GMT samples were more turbulent than those of sole ingredients, indicating the possible interaction of MNPs, TNPs and GO. Similar observations and spectral data were obtained in previous studies [34–35]. On the other hand, obtained FTIR spectra exhibited certain differences between different GO:MNPs:TNPs ratios. Specifically, the OH groups' signal at ~3400 cm^{-1} was highest in GMT 211 sample, while it was relatively weak in the other two. This could be explained that the higher GO proportion in GMT 211 sample led to the increase in the number of free OH groups, hence the more obvious FTIR signal obtained. Secondly, signals of Fe–O and Ti–O bonds at ~700–~600 cm^{-1} were clearer in GMT 111 sample than GMT 211 and GMT 212 ones, indicating that the augmentation of TiO_2 or GO proportion exerted certain influence on chemical bonds between GO, MNPs and TNPs in nanocomposites.

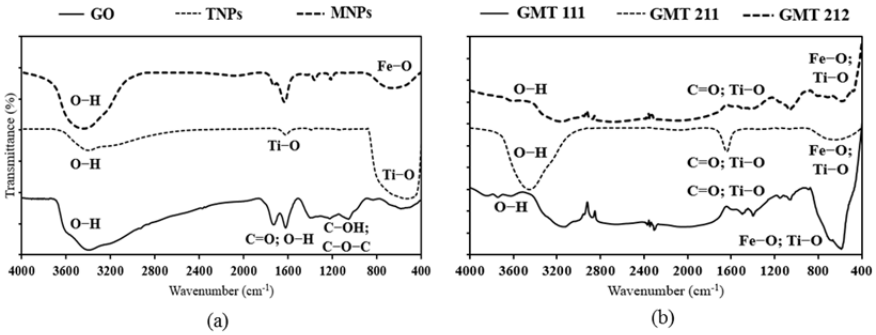

Figure 1. FTIR spectra of bare components (a) and GMT nanocomposites (b), with pointed crucial chemical bonds.

Interaction between GO, MNPs and TNPs was observed more profoundly in XRD diffractogram (Figure 2). TiO_2's signals in all GMT nanocomposite samples corresponded well with those of the anatase phase [35]. In comparison with bare ingredients and physical mixtures, these signals, specifically peaks at 2θ 38^o (004); 54^o (105); 55^o (211); 69^o (116) and 70^o (220), became weaker and broader, hence certain distortion in TiO_2's structure. In addition, signals of Fe_3O_4 nanoparticles (at 2θ 30^o (211); 35^o (311); 43^o (400); 57^o (511); 63^o (440) [36]) were present clearly in all GMT samples and they were slightly weaker to those of sole magnetite and physical samples. This resulted in our inference that Fe_3O_4@TiO_2 nanocomposite were formed, although the TiO_2 coating was probably thin [35,37]. Noticeably, signal of GO at 2θ 10.5^o (001) was absent in all GMT samples, which was different from that of physical mixtures. It could be inferred from this result that Fe_3O_4@TiO_2 nanoparticles were attached on GO sheets, hence the diminution of its peak. Similar trend was observed in Yang's publication [36]. Moreover, in common with the FTIR spectra, XRD patterns of GMT samples were more turbulent than those of bare components and physical mixtures, reinforcing our prediction that Fe_3O_4@TiO_2 nanoparticles were formed and they interacted with GO sheets. Apart from GO, signals of Fe_3O_4 and TiO_2 increased as their proportion in GMT sample augmented. In addition, the whole spectra became more turbulent, hence more defects in their structures.

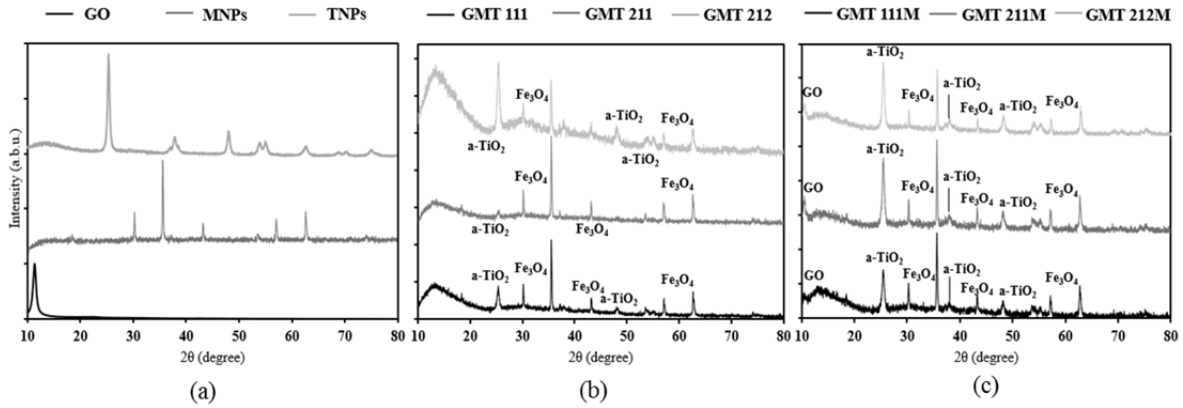

Figure 2. XRD patterns of bare components (a), nanocomposites (b), and physical mixtures (c), with pointed crucial signals (a-TiO_2: anatase TiO_2).

The UV-Vis adsorption spectra (Figure 3) almost assured the interaction between GO, Fe_3O_4 and TiO_2, because of the obvious differences in the GMT samples' spectra and those of bare components. The spectra of all GMT samples were very similar to each other in overall and the adsorption peak at ~270 nm exhibited a slight red-shift and a slight broadening as the GO and TiO_2 proportions augmented, of which possible cause was the bonding between TiO_2, Fe_3O_4 and GO. Similar trend was observed in Thongpool's publication [28].

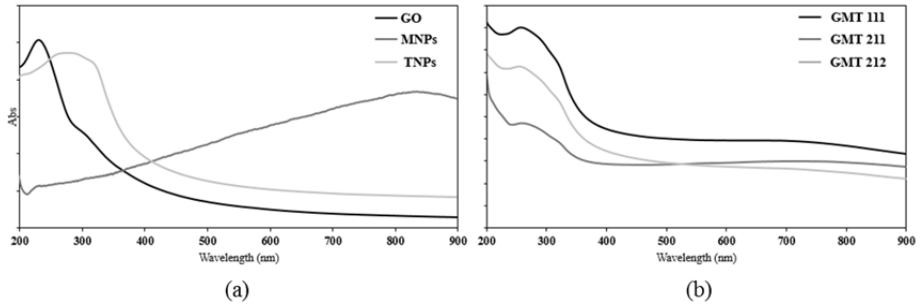

Figure 3. UV-Vis adsorption spectra of nanocomposites (a) and bare components (b).

It was obvious in Table 1 that all GMT nanocomposites possessed much lower surface area, pore volume and pore size than GO, indicating the assemblage of Fe_3O_4@TiO_2 particles on GO's surface. Secondly, the diminution in pore size of GMT nanocomposites was not as much as the pore volume and surface area, of which cause was the scattered distribution of Fe_3O_4@TiO_2 particles on GO sheets. Thirdly, the higher GO proportion in GMT nanocomposites resulted in the decrease in surface area, pore size and pore volume, indicating the possibility of GO's wrapping the Fe_3O_4@TiO_2 particles. The vibrating-sample magnetometric results (Table 2) indicated that TiO_2 nanoparticles wrapped the Fe_3O_4 nanoparticles, because of the diminution in all three paramagnetic factors. In addition, the higher GO proportion in GMT nanocomposites led to the higher possibility for Fe_3O_4 nanoparticles to be assembled directly on the surface of GO, hence the increase in paramagnetic factors.

Table 1. Specific surface area, pore size and pore volume results for GMT nanocomposites and bare GO sheets.

Sample	Specific surface area ($m^2 \cdot g^{-1}$)	Pore volume ($cm^3 \cdot g^{-1}$)	Pore size (nm)
GMT 211	34 ± 1	0.15 ± 0.01	19 ± 1
GMT 111	38 ± 1	0.19 ± 0.01	21 ± 1
GMT 212	48 ± 1	0.18 ± 0.01	17 ± 1
GO	565 ± 17	3.76 ± 0.11	30 ± 1

Table 2. Vibrating-sample magnetometric (VSM) results of nanocomposites and bare Fe_3O_4 nanoparticles.

Sample	Remanent magnetization ($emu \cdot g^{-1}$)	Maximum magnetization ($emu \cdot g^{-1}$)	Saturation magnetization ($emu \cdot g^{-1}$)
GMT 211	7.28 ± 0.22	51.16 ± 1.54	51.16 ± 1.54
GMT 111	4.21 ± 0.13	35.48 ± 1.06	35.48 ± 1.06
GMT 212	5.89 ± 0.18	41.61 ± 1.25	41.61 ± 1.25
Fe_3O_4	10.18 ± 0.31	77.04 ± 2.31	77.04 ± 2.31

SEM images (Figure 4) indicated that Fe_3O_4@TiO_2 nanoparticles were assembled on the surface of GO sheets. In addition, some TiO_2 nanoparticles were observed to assemble directly on GO's surface. It could be inferred from these results that TiO_2 particles interacted with both Fe_3O_4 (to form core-shell nanoparticles) and GO during the synthesis procedure. Because some TiO_2 particles were assembled directly on GO sheets, the amount of TiO_2 wrapping Fe_3O_4 nanoparticles diminished, hence the thin coating of these particles. This result corresponded well with the above-mentioned XRD data. On the other hand, image of TiO_2 particles on GO sheets was clearest in GMT 212 sample, with the highest TiO_2 proportion, indicating that the increase in TiO_2 ratio resulted in the higher possibility of direct assemblage of these particles on GO's surface.

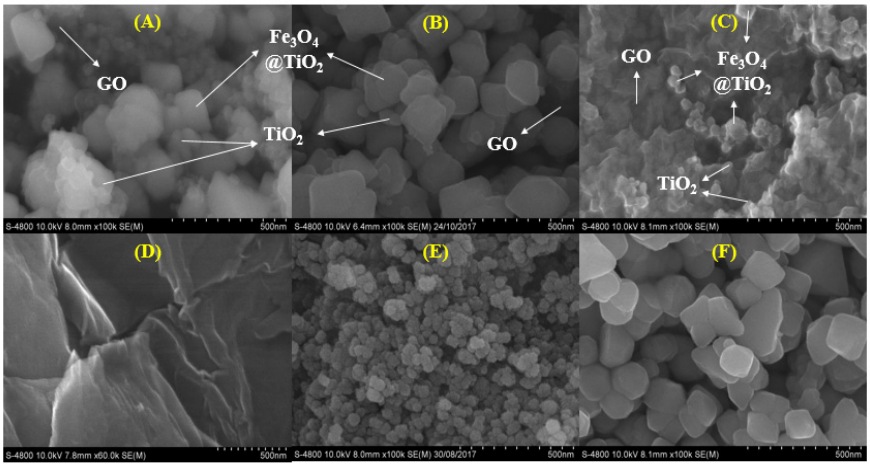

Figure 4. SEM images of GMT 111 (a), GMT 211 (b), and GMT 212 (c), with components pointed; GO (d); TiO_2 nanoparticles (e) and Fe_3O_4 nanoparticles (f).

Our statements on the distribution of Fe_3O_4@TiO_2 and TiO_2 nanoparticles on GO's surface were reinforced by TEM images (Figure 5). In addition, it was observed on these images that the increase of GO proportion in GMT nanocomposite resulted in the overlaying of those sheets on Fe_3O_4@TiO_2 and TiO_2 nanoparticles, hence darker obtained image of GMT 211 sample.

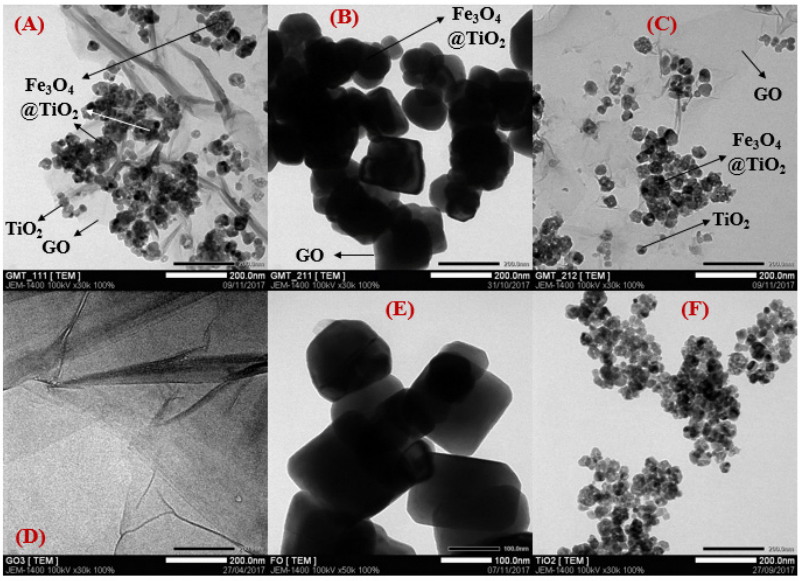

Figure 5. TEM images of GMT 111 (a), GMT 211 (b), and GMT 212 (c), with components pointed, GO (d), Fe_3O_4 nanoparticles (e) and TiO_2 nanoparticles (f).

3.2. Photocatalytic activity investigation

Using ICP-MS analysis, proportion (wt%) of atomic Fe and Ti were determined. Subsequently, proportion of Fe_3O_4, TiO_2, and GO, were calculated (Table 3). The highest proportion value of each component were applied for the appropriate amount of bare GO, Fe_3O_4, and TiO_2 for RhB photodegradation experiments.

Table 3. Proportion (wt%) of Fe, Ti, Fe_3O_4, TiO_2 and GO in GMT nanocomposites.

Sample	Proportion (wt%)				
	Fe	Ti	Fe_3O_4	TiO_2	GO
GMT 111	32.0	23.6	44.2	39.4	16.4
GMT 211	40.5	25.8	55.9	43.1	1.0
GMT 212	36.3	20.3	50.2	33.8	16.0

Rhodamine B (RhB) dye photodegradation of GMT and bare components samples were conducted in 1 h of natural sunlight exposure. Data were presented as means ± standard error mean, with statistically significant difference ($\alpha = 0.05$). The obtained results were shown in Table 4. The photocatalytic decolouration of pure Fe_3O_4 is only 24.1% after 1 h exposing under sunlight. Interestingly, when Fe_3O_4 was combined with GO and TiO_2 to form the tertiary nanocomposite GMT, its photocatalytic activity enhances significantly ($p < 0.05$). The decolouration efficacy of GMT 111

is increase 6.2 % as compared to pure Fe_3O_4, proposing that GO and TiO_2 might reduce the high charge recombination rate of Fe_3O_4. In order words, the electron (e^-) and hole (h^+) from the valence band creating by Fe_3O_4 could migrate into GO sheet leading to hinder the disadvantage of Fe_3O_4; consequently, increase the photoelectrocatalytic performance than pure Fe_3O_4. The result of GMT 211 is further confirmed this proposal. The higher amount of GO in GMT 211 obviously increases the decolouration efficiency of RhB by 38.6% which is 1.5 times as compared to GMT 111 ($p = 4.05E\text{-}21 < 0.05$). Moreover, the higher amount of GO/TiO_2 to Fe_3O_4 (GMT 212) also promotes the decolouration ability of RhB, leading to an increase from 25.6% (GMT 111) to 52.9%. It is clear that the introduction of TiO_2 can significantly increase the amount RhB degradation. The decolouration performance of GMT nanocomposite increase in the order: GMT 111 < GMT 211 < GMT 212, which is followed the same trend as the increment in specific surface area and as the decrease in pore size. Therefore, the maximum was observed for GMT 212 nanocomposite, which might be due to the adsorption of RhB dye as the catalyst has large surface area support. In this study, we proposed that the Fe_3O_4@TiO_2 particles assembled on GO sheets blocked these pores, hence increase the separation of photogenerated electrons-holes pair (e^-h^+) significantly, resulting in an increase in the number of electrons/holes participating in the photodegradation process.

Table 4. Decolouration efficiency (D, %) of nanocomposites and separate ingredients.

Sample	GO:Fe_3O_4:TiO_2 weight ratios	C value ($mg \cdot L^{-1}$)	C_o value ($mg \cdot L^{-1}$)	D (%)
GMT 111	1:1:1	7.44 ± 0.01	10	25.6 ± 0.08
GMT 211	2:1:1	6.14 ± 0.01	10	38.6 ± 0.08
GMT 212	2:1:2	4.71 ± 0.01	10	52.9 ± 0.08
GO	-	4.78 ± 0.01	10	52.2 ± 0.08
Fe_3O_4	-	7.59 ± 0.01	10	24.1 ± 0.08
TiO_2	-	7.28 ± 0.01	10	27.2 ± 0.08

It was noticeable in Table 4 that bare GO caused greater diminution of RhB concentration than the GMT 111 and GMT 211 samples and almost equal to the GMT 212 sample. GO itself possesses very high specific surface area, pore size and pore volume (Table 1), hence its good capability of absorbing RhB molecules. Unlike TiO_2, GO does not possess photocatalytic activity. It is, therefore, probable that the decrease of RhB concentration after photodegradation in GO sample actually resulted from the absorption of RhB molecules on GO's surface, rather than the photodegradation reaction. In order to verify the manner in which RhB concentration decreased, the sole RhB solution and obtained RhB solutions of GMT samples were passed to HPLC analysis, using a UV-Vis adsorption detector, and the obtained chromatographs were shown in Figure 6. From these results, it was obvious that the photodegrading reaction on RhB dye caused by GMT nanocomposite actually occurred, due to the presence of "non-RhB" peaks at retention times of 5, 6.3, 6.5, and 6.7 min, and the diminution of RhB peak at retention time of 9.5 min. These considerations have led to our statement that despite possessing the highest decolouration efficiency, GO did not actually degrade RhB dye molecules.

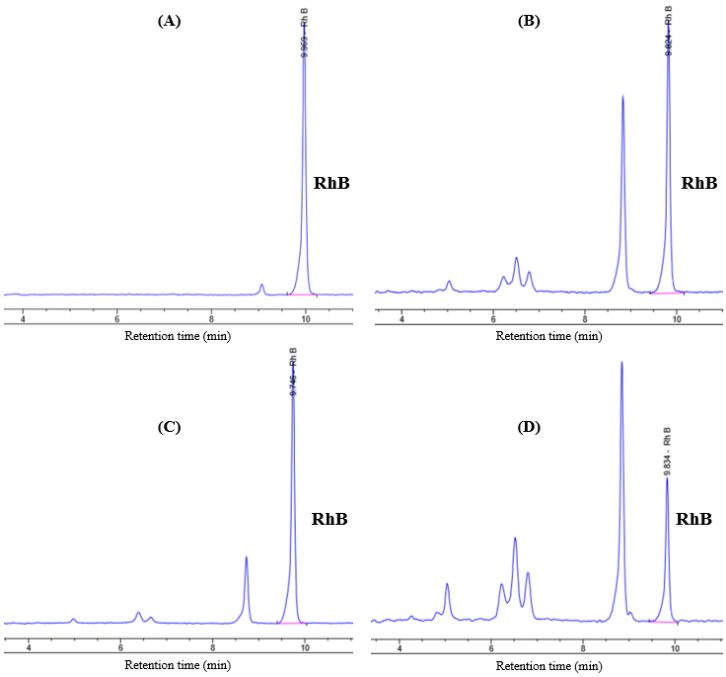

Figure 6. HPLC graphs of sole RhB solution (a) and that of GMT 111 (b), GMT 211 (c) and GMT 212 (d).

4. Conclusion

In this work, Fe_3O_4@TiO_2-GO nanocomposite material was successfully synthesized. Its morphological character was the assemblage of Fe_3O_4@TiO_2 and TiO_2 nanoparticles on GO's surface. The synthesized nanocomposite were easy to be collected and exhibited higher photocatalytic activity than bare components of Fe_3O_4 and TiO_2. GO:Fe_3O_4:TiO_2 ratio's effect on the nanocomposite's properties was also investigated and led to our statement that the increase of TiO_2 amount resulted in the higher possibility of direct assemblage of TiO_2 nanoparticles on GO's surface and the higher photocatalytic activity. In addition, the increase of GO amount can cause overlaying on nanoparticles of the nanocomposite. From the angle of dye photodegradation, Fe_3O_4@TiO_2-GO nanocomposite showed high potential for wastewater purification and other photocatalytic applications.

Acknowledgments

This research is funded by Vietnam National Foundation for Science and Technology Development (NAFOSTED) under grant number 104.03-2017.49 and by Vietnam Academy of Science and Technology (VAST) under grant number VAST.ĐLT.06/16-17.

Conflict of interests

The authors declare no competing financial interest.

References

1. Eckert H, Bobeth M, Teixeira S, et al. (2015) Modeling of photocatalytic degradation of organic components in water by nanoparticle suspension. *Chem Eng J* 261: 67–75.
2. Martins PM, Ferreira C, Silva A, et al. (2018) TiO_2/graphene and TiO_2/graphene oxide nanocomposites for photocatalytic applications: A computer modeling and experimental study. *Compos Part B-Eng* 145: 39–46.
3. Luo Y, Guo W, Ngo HH, et al. (2014) A review on the occurrence of micropollutants in the aquatic environment and their fate and removal during wastewater treatment. *Sci Total Environ* 473: 619–641.
4. Raghavan N, Thangavel S, Sivalingam Y, et al. (2018) Investigation of photocatalytic performances of sulfur based reduced graphene oxide-TiO_2 nanohybrids. *Appl Surf Sci* 449: 712–718.
5. Anandan S, Ikuma Y, Niwa K (2010) An overview of semi-conductor photocatalysis: modification of TiO_2 nanomaterials. *Solid State Phenom* 162: 239–260.
6. Coelho LL, Hotza D, Estrella AS, et al. (2019) Modulating the photocatalytic activity of TiO_2 (P25) with lanthanum and graphene oxide. *J Photoch Photobio A* 372: 1–10.
7. Timoumi A, Alamri SN, Alamri H (2018) The development of TiO_2-graphene oxide nano composite thin films for solar cells. *Results Phys* 11: 46–51.
8. Chen C, Cai W, Long M, et al. (2010) Synthesis of visible-light responsive graphene oxide/TiO_2 composites with p/n heterojunction. *ACS Nano* 4: 6425–6432.
9. Rambabu Y, Kumar U, Singhal N, et al. (2019) Photocatalytic reduction of carbon dioxide using graphene oxide wrapped TiO_2 nanotubes. *Appl Surface Sci* 485: 48–55.
10. Rambabu Y, Jaiswal M, Roy SC (2015) Enhanced photoelectrochemical performance of multi-leg TiO_2 nanotubes through efficient light harvesting. *J Phys D Appl Phys* 48: 295302.
11. Kozlova EA, Vorontsov AV (2006) Noble metal and sulfuric acid modified TiO_2 photocatalysts: Mineralization of organophosphorous compounds. *Appl Catal B-Environ* 63: 114–123.
12. Wu MC, Huang WK, Lin TH, et al. (2019) Photocatalytic hydrogen production and photodegradation of organic dyes of hydrogenated TiO_2 nanofibers decorated metal nanoparticles. *Appl Surface Sci* 469: 34–43.
13. Marschall R, Wang L (2014) Non-metal doping of transition metal oxides for visible-light photocatalysis. *Catal Today* 225: 111–135.
14. Martins P, Gomez V, Lopes A, et al. (2014) Improving photocatalytic performance and recyclability by development of Er-doped and Er/Pr-codoped TiO_2/poly(vinylidene difluoride)–trifluoroethylene composite membranes. *J Phys Chem C* 118: 27944–27953.
15. Almeida NA, Martins PM, Teixeira S, et al. (2016) TiO_2/graphene oxide immobilized in P (VDF-TrFE) electrospun membranes with enhanced visible-light-induced photocatalytic performance. *J Mater Sci* 51: 6974–6986.
16. Yusoff AHM, Salimi MN, Jamlos MF (2017) A review: Synthetic strategy control of magnetite nanoparticles production. *Adv Nano Res* 6: 1–19.
17. Hossain MT, Hossain MM, Begum MHA, et al. (2018) Magnetite (Fe_3O_4) nanoparticles for chromium removal. *Bangladesh J Sci Ind Res* 53: 219–224.
18. Smith AT, LaChance AM, Zeng S, et al. (2019) Synthesis, properties, and applications of graphene oxide/reduced graphene oxide and their nanocomposites. *Nano Mater Sci* 1: 31–47.

19. Cui Y, Kundalwal S, Kumar S (2016) Gas barrier performance of graphene/polymer nanocomposites. *Carbon* 98: 313–333.
20. Gebrezgiabher M, Gebreslassie G, Gebretsadik T, et al. (2019) A C-doped TiO_2/Fe_3O_4 nanocomposite for photocatalytic dye degradation under natural sunlight irradiation. *J Compos Sci* 3: 1–11.
21. Ma P, Jiang W, Wang F, et al. (2013) Synthesis and photocatalytic property of $Fe_3O_4@TiO_2$ core/shell nanoparticles supported by reduced graphene oxide sheets. *J Alloy Compd* 578: 01–506.
22. Stefan M, Pana O, Leostean C, et al. (2014) Synthesis and characterization of Fe_3O_4–TiO_2 core-shell nanoparticles. *J Appl Phys* 116: 114312.
23. Xin T, Ma M, Hepeng Z, et al. (2014) A facile approach for the synthesis of magnetic separable $Fe_3O_4@TiO_2$, core–shell nanocomposites as highly recyclable photocatalysts. *Appl Surface Sci* 288: 51–59.
24. Tan L, Zhang X, Liu Q, et al. (2015) Synthesis of $Fe_3O_4@TiO_2$ core–shell magnetic composites for highly efficient sorption of uranium (VI). *Colloid Surface A* 469: 279–286.
25. Liang Y, He X, Chen L, et al. (2014) Preparation and characterization of TiO_2-graphene@Fe_3O_4 magnetic composite and its application on the removal of trace microcystin-LR. *RSC Adv* 4: 56883–56891.
26. Cruz M, Gomez C, Duran-Valle CJ, et al. (2017) Bare TiO_2 and graphene oxide TiO_2 photocatalysts on the degradation of selected pesticides and influence of the water matrix. *Appl Surface Sci* 416: 1013–1021.
27. Sharma M, Behl K, Nigam S, et al. (2018) TiO_2-GO nanocomposite for photocatalysis and environmental applications: A green synthesis approach. *Vacuum* 156: 434–439.
28. Thongpool V, Phunpueok A, Jaiyen S (2018) Preparation, characterization and photocatalytic activity of ternary graphene-Fe_3O_4:TiO_2. *Dig J Nanomater Bios* 13: 499–504.
29. Hummers Jr WS, Offeman RE (1958) Preparation of graphitic oxide. *J Am Chem Soc* 80: 1339.
30. Marcano DC, Kosynkin DV, Berlin JM, et al. (2010) Improved synthesis of graphene oxide. *ACS nano* 4: 4806–4814.
31. Emiru TF, Ayele DW (2017) Controlled synthesis, characterization and reduction of graphene oxide: A convenient method for large scale production. *Egypt J Basic Appl Sci* 4: 74–79.
32. Manalu SP, Natarajan TS, De Guzman M, et al. (2018) Synthesis of ternary g-$C_3N_4/Bi_2MoO_6/TiO_2$ nanotube composite photocatalysts for the decolorization of dyes under visible light and direct sunlight irradiation. *Green Process Synth* 7: 493–505.
33. Bordbar AK, Rastegari AA, Amiri R, et al. (2014) Characterization of modified magnetite nanoparticles for albumin immobilization. *Biotechnol Res Int* 2014: 705068.
34. Benjwal P, Kumar M, Chamoli P, et al. (2015) Enhanced photocatalytic degradation of methylene blue and adsorption of arsenic(III) by reduced graphene oxide (rGO)–metal oxide (TiO_2/Fe_3O_4) based nanocomposites. *RSC Adv* 5: 73249–73260.
35. Zheng K, Zhang T, Lin P, et al. (2015) 4-Nitroaniline degradation by TiO_2 catalyst doping with manganese. *J Chem* 2015: 382376.
36. Yang X, Chen W, Huang J, et al. (2015) Rapid degradation of methylene blue in a novel heterogeneous Fe_3O_4@rGO@TiO_2-catalyzed photo-Fenton system. *Sci Rep* 5: 10632.

37. Khashan S, Dagher S, Tit N, et al. (2017) Novel method for synthesis of Fe_3O_4@TiO_2 Core/Shell Nanoparticles. *Surf Coat Tech* 322: 92–98.